International Journal Of
Industrial Electronics Control and Optimization
Print ISSN: 3517-2645
Online ISSN: 3568-2645
Homepage: https://ieco.usb.ac.ir/

Motion Shape Control of Superstructure in Base-Isolated Tall Buildings using GBMO-Based Uniform Deformation Techniques

Sadegh Etedali[1]

[1]Department of Civil Engineering, Birjand University of Technology, P.O. Box 97175-569, Birjand, Iran
[1]Corresponding author's email: etedali@birjandut.ac.ir

Article Info

Article type:
Research Article

Article history:
Received: 16-September-2024
Received in revised form: 10-November-2024
Accepted: 27-November-2024
Published online: 22-June-2025

Keywords:
Base-isolated structure,
GBMO algorithm,
Motion shape control,
Seismic performance,
Tall building

ABSTRACT

This paper proposes three techniques aimed at enhancing the seismic performance of base-isolated tall buildings through uniform deformation of the superstructure. The first and second methods focus on generating a uniform modal shape and an even distribution of seismic loads across the floors, while the third method seeks to minimize the standard deviation of story drifts. For these purposes, an optimization procedure based on a gas Brownian motion optimization (GBMO) algorithm is defined. Simulation results, compared to those for a 20-story reference base-isolated structure, demonstrate that these techniques effectively reduce maximum floor displacement, particularly in the upper levels of the studied buildings. The proposed methods show clear advantages in lowering maximum floor drift, a critical factor in seismic damage. Specifically, methods 1 and 3 resulted in significant reductions in maximum floor drift, ranging from 30% to 80% in the upper floors. Additionally, these methods led to a reduction of 10% to 15% in maximum acceleration and seismic forces on the upper floors, while a slight increase was observed in the lower floors. Among the methods, method 1 exhibited the best overall performance, yielding average reductions of 6.65%, 32.65%, and 0.88% in maximum floor displacement, drift, and acceleration, respectively, when compared to the reference base-isolated structure. While methods 2 and 3 resulted in only modest reductions in displacement and acceleration, they were effective in significantly lowering maximum floor drift.

I. Introduction

Base isolation is an engineering technique to protect structures from the damaging effects of earthquake excitations. Decoupling the structure from ground motion, significantly reduces the seismic forces transmitted to the structure, thereby enhancing its resilience and safety during an earthquake. This method has been increasingly adopted in the design and retrofit of both new and existing structures, particularly in regions prone to seismic activity [1]. Base isolation systems were initially designed for short-period structures, such as low-rise buildings, which are subjected to short-period ground motions, like those from far-field earthquakes. The use of base isolation techniques shifts the fundamental period of typical low-rise buildings to 2.0–3.0 seconds, thereby significantly reducing seismic force demands during far-field ground motions and the spectral acceleration decreases. However, However, the concerns regarding the application of base isolation systems in high-rise buildings arise primarily from the relatively long fundamental period of the fixed-base superstructure [2-3]. Although the seismic performance of base isolation in tall buildings may not be as pronounced as those observed in short-period structures, they are still significant when compared to the improvements achieved in the response of long-period structures using some well-established seismic protection systems [3]. Over the last decade, the 18-story office Sendai MT building, the 41-story Thousand Tower, and a super high-rise building with a height of 177.4 m are some examples of utilizing the base isolations in tall buildings [2-3]. Furthermore, several studies have been carried out on base-isolated high-rise buildings. Roussis and Constantinou [4] introduced innovative devices designed to address the damage caused by the uplift of isolators during significant earthquakes. Ariga et al. [5] examined the resonant behavior of these buildings under long-period

Copyright © S. Etedali
Publisher: University of Sistan and Baluchestan

ground motions, highlighting critical vulnerabilities. Hino et al. [6] employed the Monte Carlo method to evaluate the limitations on the height-to-width ratio for base-isolated buildings, ensuring their stability. Ma et al. [7] Studied the seismic response of base-isolated tall buildings under fully nonstationary excitation. The effects of stiffness of a base-isolation layer and a superstructure for a base-isolated high-rise building were studied in [8]. Darwish and Bhandari [9] investigated the seismic performance of two 12-story and 15-story base-isolated steel–concrete composite buildings equipped with lead rubber bearing isolators. Li et al [10] conducted a comprehensive investigation on the reduced model and the seismic response of the inter-story isolated building.

In recent years, metaheuristic optimization algorithms have garnered significant attention from researchers for the optimal design of seismic isolators in structures subjected to earthquakes. Shourestani et al. [11] applied a particle swarm optimization algorithm for seismic control of a smart base-isolated structure considering soil-structure interaction effects. Pal et al. [12] employed a genetic algorithm to optimize base isolation parameters across various soil conditions, including hard, medium, and soft soils. Etedali et al. [13] addressed the optimal design of pure-friction isolators with restoring devices in seismic-excited structures using a multi-objective cuckoo search-based approach. Ockak et al. [14] conducted a comprehensive study on the optimization of seismic isolators at the base of structures, using an adaptive harmony search algorithm. Öncü-Davas [15] explored various metaheuristic approaches for optimizing non-linear base isolation systems under near-fault earthquakes, considering the flexibility of the superstructure. Etedali and Khosravi Kareshk [16] proposed two optimal isolator distributions in the base story of asymmetric base-isolated structures to reduce torsional responses. Lastly, Lei and Yang [17] proposed an improved method for stochastic optimization of electromagnetic inertial mass dampers in nonlinear hybrid isolation systems subject to seismic excitations.

Base isolators are known to significantly reduce spectral acceleration by increasing the fundamental period of the structure. Optimal seismic isolation performance is achieved when the superstructure behaves as a rigid body, making base isolators particularly effective for low-rise structures with greater rigidity. This results in substantial reductions in inter-story displacements and absolute acceleration of the superstructure floors. Conversely, as the number of floors and the flexibility of the superstructure increase, the response of the base-isolated structure becomes increasingly influenced by the superstructure's lateral movements and interactions. In such scenarios, the effectiveness of seismic isolation in controlling inter-story drift and absolute floor acceleration generally diminishes. However, the motion shape of the superstructure can be controlled through the optimal design of floor stiffness, employing an optimization process to achieve uniform deformation across the superstructure. This technique aims to create an ideal state of isolation for the structure. This study proposes three uniform deformation techniques based on the GBMO algorithm to enhance the seismic performance of base-isolated tall buildings. Numerical analyses were conducted on a 20-story base-isolated building, and the seismic performances of these three proposed techniques were compared.

The structure of the paper is as follows. Section 2 introduces the equation of motion for the nonlinear base-isolated structures. Section 3 presents three methodologies for seismic performance enhancement of base-isolated tall buildings. An overview of the GBMO algorithm is provided in Section 4. Section 5 includes a numerical study on a 20-story base-isolated structure. The simulation results are discussed in Section 6. The paper concludes with a summary of the findings in the end section.

II. Equation of Motion for Nonlinear Base-Isolated Structures

The mathematical representation of the motion for a base-isolated structure under the ground acceleration $\ddot{x_g}(t)$ is expressed as [18]:

$$M\ddot{\mathrm{u}}(t) + \mathrm{C}\dot{\mathrm{u}}(t) + \mathrm{Ku}(t) + \Lambda \mathrm{f}(t) = -\mathrm{M1}\ddot{x_g}(t) \quad (1)$$

Here, M, C, and K denote the mass, damping, and stiffness matrices of the structure, respectively. Also, t is the duration of the ground acceleration. The terms $\mathrm{u}(t)$, $\dot{\mathrm{u}}(t)$, and $\ddot{\mathrm{u}}(t)$ represent the vectors of relative displacement, velocity, and acceleration of the base story and superstructure floors relative to the ground. The vector 1 indicates the location of the earthquake, Λ is the vector corresponding to the location of the isolation system and $\mathrm{f}(t)$ represents the restoring force of the isolation system. The restoring force of a lead rubber bearing (LRB) as a well-known isolation system can be calculated as:

$$\mathrm{f}(t) = Q_{pb} + \mathrm{k}_1 x_1(t) + c_1 \dot{\mathrm{x}}_1(t) \quad (2)$$

In this context, Q_{pb} represents the yield force of the lead plug, while k_1 and c_1 denote the linearized average stiffness of the nonlinear force-displacement loop of LRB and the viscous coefficient of the linearized LRB damping, respectively. The terms $x_1(t)$ and $\dot{x}_1(t)$ correspond to the relative displacement and velocity across the bearing. The yield force of the lead plug can be expressed as follows:

$$Q_{pb} = (1 - k_{yield}/k_{initial})Q_y \quad (3)$$

Here, k_{yield} and $k_{initial}$ are the post-yield and initial shear

stiffness, respectively, and Q_y represents the yield force arising from both the lead plug and rubber stiffness. While the nonlinear behavior of the LRB can be modeled using a bilinear approach, this model tends to overestimate the acceleration responses of the structure. To address this issue, the Bouc-Wen model, which better aligns with experimental results, can be employed. In this model, the hysteretic force component Q_{hyst} is defined as:

$$Q_{hyst} = Q_{pb}\, z(t) \tag{4}$$

The evolutionary variable z can be described by the differential equation:

$$\dot{z}(t) = A\dot{x}_1(t) - \gamma z(t)|\dot{x}_1(t)||z(t)|^{n-1} - \beta\dot{x}_1(t)|z(t)|^n \tag{5}$$

where $n = 1$, and the parameters $A = 2\gamma = 2\beta = k_{intial}/Q_y$ define the shape of the hysteresis loop.

III. Methodology

An optimization problem is formulated to determine the optimal distribution of the superstructure's stiffness along its height, ensuring that the superstructure behaves like a rigid body. This is achieved by seeking a more uniform deformation of the superstructure compared to the original structure, which can be addressed using the following methods:

A. Method 1

The first method involves identifying a stiffness distribution along the height of the superstructure that results in a uniform modal shape. The standard deviation of the first mode shape vector, denoted as σ_φ is given by:

$$\sigma_\varphi = \sqrt{\frac{1}{N+1}\sum_{i=1}^{N+1}(\varphi_{i1} - \bar{\varphi}_1)^2} \tag{6}$$

where N is the number of structural floors, $\varphi_{i1}$is the ith element of the first mode shape vector, and $\bar{\varphi}_1$ is the mean of the first mode shape vector, defined as:

$$\bar{\varphi}_1 = \frac{1}{N+1}\sum_{i=1}^{N+1}\boldsymbol{\varphi}_{i1} \tag{7}$$

By considering the ratio of the standard deviation of the first mode shape vector of the structure relative to that of the original structure as the cost function J_1 , the following optimization problem is formulated to achieve a uniform deformation of the superstructure:

$$\begin{aligned} &\text{Find:} && k_s = \{k_2, k_3, \dots, k_{N+1}\} \\ &\text{Minimize:} && J_1 = \frac{\sigma_\varphi}{\widetilde{\sigma_\varphi}} \\ &\text{Subjected to:} && k_{s-min} \ll k_s \ll k_{s-max} \end{aligned} \tag{8}$$

where k_s represents the design vector of the stiffness coefficients for the superstructure's floors, and k_{s-min} and k_{s-max} are the lower and upper bounds of the design vector.

B. Method 2

The second method seeks to find a stiffness distribution along the height of the superstructure that ensures a uniform distribution of seismic loads across the floors. The optimization problem is defined as follows:

$$\begin{aligned} &\text{Find:} && k_s = \{k_2, k_3, \dots, k_{N+1}\} \\ &\text{Minimize:} && J_2 = \frac{\sigma_f}{\widetilde{\sigma_f}} \\ &\text{Subjected to:} && k_{s-min} \ll k_s \ll k_{s-max} \end{aligned} \tag{9}$$

where σ_f represents the standard deviation of the seismic forces applied to the structure, calculated by:

$$\sigma_f = \sqrt{\frac{1}{N+1}\sum_{i=1}^{N+1}(\max(f_i(t)) - \bar{f}(t))^2} \tag{10}$$

Here, max $(f_i(t))$ is the maximum force on the i–th floor, and $\bar{f}$(t) is the mean of the maximum forces across the floors, given by:

$$\bar{f} = \frac{1}{N+1}\sum_{i=1}^{N+1}\max(f_i(t)) \tag{11}$$

Additionally, $\widetilde{\sigma_f}$ denotes the corresponding standard deviation of the seismic forces applied to the original structure.

C. Method 3

To achieve a rigid body-like behavior in the superstructure, the standard deviation of the story drifts σ_d is minimized through the following optimization problem:

$$\begin{aligned} &\text{Find:} && k_s = \{k_2, k_3, \dots, k_{N+1}\} \\ &\text{Minimize:} && J_3 = \frac{\sigma_d}{\widetilde{\sigma_d}} \\ &\text{Subjected to:} && k_{s-min} \ll k_s \ll k_{s-max} \end{aligned} \tag{12}$$

where

$$\sigma_d = \sqrt{\frac{1}{N+1}\sum_{i=1}^{N+1}(\max(d_i(t)) - \bar{d}(t))^2} \quad (13)$$

$$\bar{d} = \frac{1}{N+1}\sum_{i=1}^{N+1}\max(d(t)_i) \quad (14)$$

In these expressions, $\max(d_i)$ denotes the maximum drift of the i–th, and $\bar{d}$ is the average maximum drift across all floors. The term $\widetilde{\sigma_d}$ represents the corresponding standard deviation of the story drifts in the structure.

IV. Gas Brownian Motion Optimization

The GBMO algorithm is a noteworthy addition to the suite of metaheuristic optimization methods, delivering strong performance in traversing complex search spaces. It is introduced by Abdechiri et al. [19]. The GBMO leverages the physical principles of gas molecule dynamics, specifically their Brownian motion and turbulent rotational movement. This algorithm is designed to tackle complex optimization challenges by thoroughly exploring the search space to locate global optima. The GBMO algorithm has found applications in various domains where intricate optimization problems are common, including engineering design, machine learning, and operations research. Its capability to avoid local optima and effectively search for global solutions makes it particularly useful in situations where conventional optimization techniques may fall short. In this approach, the positions of molecules symbolize potential solutions within the search space. As these molecules move, their collective actions guide the process toward the global optimum. In the GBMO, each molecule is characterized by four primary attributes: position, mass, velocity, and turbulent radius. The algorithm follows these steps [19]:

1. Gas molecules are randomly generated within the search space.
2. Each molecule is assigned a random radius within the range [0, 1].
3. The system temperature is initialized, acting as a convergence criterion. The temperature starts high at the beginning of the optimization process and gradually decreases over time.
4. The positions and velocities of the molecules are updated according to the following equations:

$$v_i^d(t+1) = v_i^d(t) + \sqrt{\frac{3kT}{m}} \quad (15)$$

$$x_i^d(t+1) = x_i^d(t) + v_i^d(t+1) \quad (16)$$

where $x_i^d(t)$ and $v_i^d(t)$ represent the position and velocity of the ith molecule in the d-th dimension at iteration t, respectively. Additionally, T, k, and m are the temperatures, the Boltzmann constant, and the mass value associated with each molecule.

5. The fitness of each molecule's position is evaluated using the objective function.
6. In addition to Brownian motion, each molecule also undergoes turbulent rotational motion, which is generated by a chaotic sequence generator under the setting $a = 0.5$ and $b = 0.2$, described by the following equation:

$$x_i^d(t+1) = x_i^d(t) + b - \left(\frac{a}{2\pi}\right) sin(2\pi x_i^d)\, mod(1), \quad (17)$$

7. The objective function is re-evaluated, and the fitness of the molecules is compared based on their updated positions.
8. The mass and temperature of the molecules are adjusted using the following equations:

$$worst(t) = min\, fit_i(t) i \in \{1,2,..,N\} \quad (18)$$

$$best(t) = max\, fit_i(t) i \in \{1,2,..,N\} \quad (19)$$

$$m_i(t) = \frac{fit_i(t) - worst(t)}{best(t) - worst(t)} \quad (20)$$

$$T = T - \left(\frac{1}{mean(fit_i(t))}\right) \quad (21)$$

In Eq. (19), $worst(t)$ and $best(t)$ are the worst and best fitness values at iteration t, while $fit_i(t)$ represents the fitness of the ith molecule during the same iteration.

9. If the stopping criterion is met, the algorithm concludes. If not, steps 4 through 8 are repeated until the criterion is satisfied.

V. Numerical studies

To evaluate the proposed methodologies for enhancing the seismic performance of base isolation systems in tall buildings, a 20-story shear building is considered for numerical studies. The parameters of the superstructure and LRB as an isolation system are summarized in Table 1. An artificial earthquake for modeling the ground acceleration is produced using a band-limited Gaussian white noise. The well-known Kanai-Tajimi power spectral density function (PSDF) is often applied to model artificial earthquake excitations [20]. However, several attempts have been carried out to overcome the existing drawbacks in the PSDF. A second-order filter was proposed by Nagarajaiah and

Narasimhan [21] with the following PSDF:

TABLE 1 THE PARAMETERS OF THE SUPERSTRUCTURE AND LRB

Number of stories	$\boldsymbol{N = 20}$
Story mass (*i=2,..., N+1*)	$m_i = 1024$ kg
The damping ratio of the structure	$\xi_s = 5\%$
Base story mass	$m_b = 1024$ kg
The damping ratio of the LRB	$\xi_b = 10\%$
The target period of the LRB	T_b=3 sec.
Post-yield to pre-yield stiffness ratio	0.1
Yield force	$Q_y = 0.05W$

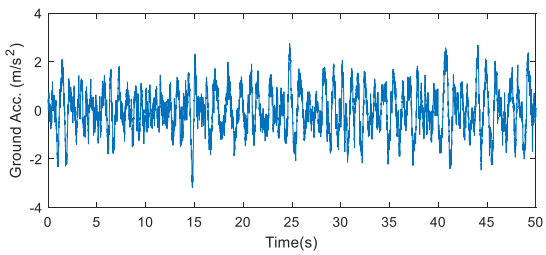


Fig. 1. The artificial earthquake excitation

$$s(\omega) = \frac{4\xi_g \omega_g \omega}{\omega^2 + 2\xi_g \omega_g \omega + \omega_g^2} \qquad (22)$$

where ξ_g and ω_g are the damping ratio and angular frequency of the ground. The above-mentioned artificial earthquake excitation was widely employed for modeling the earthquakes to apply to the base-isolated structures [22-24]. Figure 1 indicates the output of this filter which is applied to simulate the ground acceleration.

The nonlinear time-history analyses of the base-isolated structure are carried out using the MATLAB/Simulink software package [25]. Based on the optimization problem defined in section 3, the optimal floor stiffnesses are obtained using the GBMO algorithm. With an initial temperature of 30 °C and $\varepsilon = 0.001$, the GBMO algorithm with 200 gas molecules is implemented to find the optimal stiffnesses of the superstructure's floors. The convergence graphs of the GBMO algorithm for methods 1, 2, and 3 are illustrated in Figure 2. As can be seen, the convergences of the GBMO algorithm for methods 1, 2, and 3 are achieved in iterations 90, 90, and 150, respectively.

I. Results and discussion

The time responses of the fixed-base (FB) structure, the reference base-isolated (BI) structure, and the base-isolated structures designed using methods 1, 2, and 3 are compared in terms of top-floor displacement in Figure 3. Similarly, the time responses of the structures in terms of top-floor drift and top-floor acceleration are presented in Figures 4 and 5, respectively.

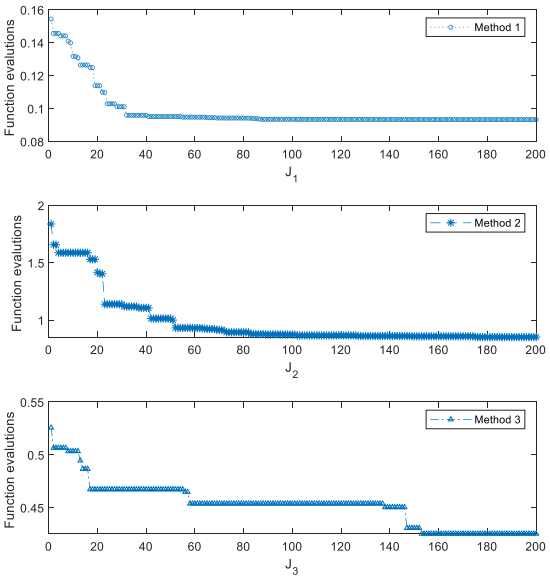


Fig. 2. The convergence graphs of the GBMO algorithm for methods 1, 2, and 3

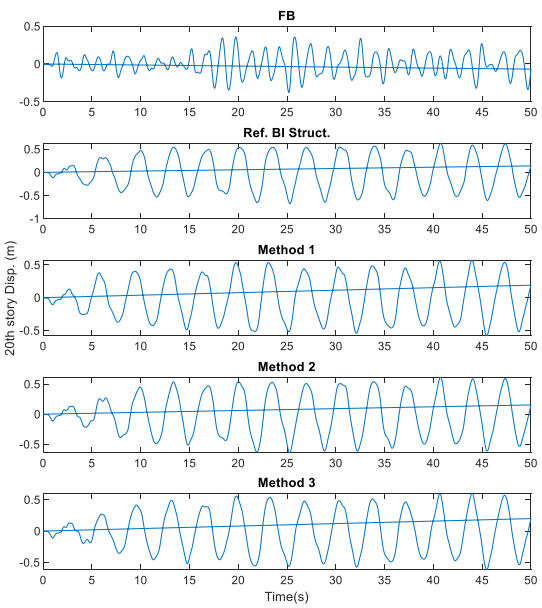


Fig. 3. Time histories of top floor displacement of the FB structure, reference BI structure, and the base-isolated structures designed using the proposed methods

As shown, the maximum top-floor displacement of the reference BI structure increases from 37.89 cm in the FB structure to 67.53 cm. Meanwhile, the maximum top-floor drift decreases from 3.46 cm to 1.65 cm, and the maximum top-floor acceleration reduces from10.58 m/s² to 4.77 m/s².

Therefore, it can be concluded that seismic isolation significantly reduces key seismic responses of the structure

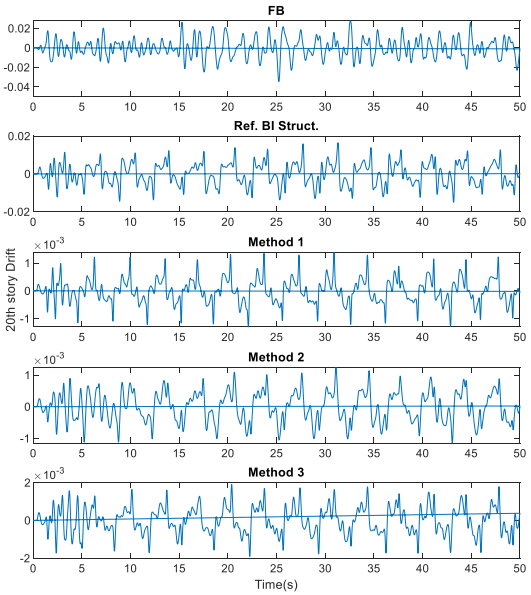


Fig. 4. Time histories of top floor drift of the FB structure, reference BI structure, and the base-isolated structures designed using the proposed methods

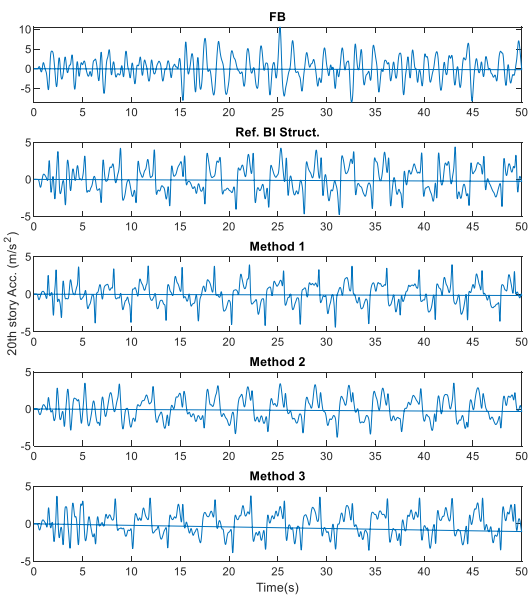


Fig. 5. Time histories of top floor acceleration of the FB structure, reference BI structure, and the base-isolated structures designed using the proposed methods

(i.e., maximum floor drift and acceleration), which often cause structural and non-structural damage. Furthermore, the proposed methods result in a notable decrease in the maximum top-floor drift compared to the reference BI structure. Specifically, the maximum top-floor drift decreases from 1.65 cm to 0.14 cm, 0.12 cm, and 0.19 cm for methods 1, 2, and 3,

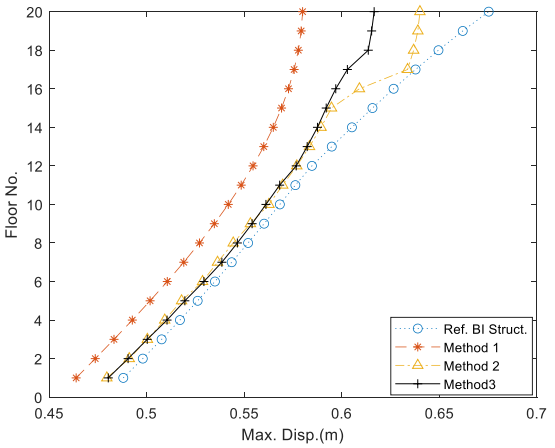


Fig. 6. Maximum floor displacements for the reference BI structure and the base-isolated structures designed using methods 1, 2, and 3.

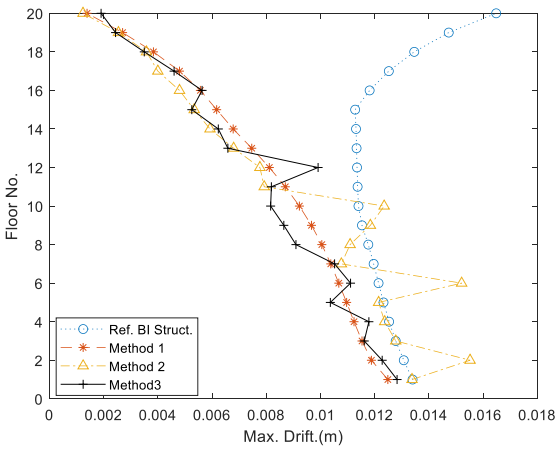


Fig. 7. Maximum floor drifts for the reference BI structure and the base-isolated structures designed using methods 1, 2, and 3

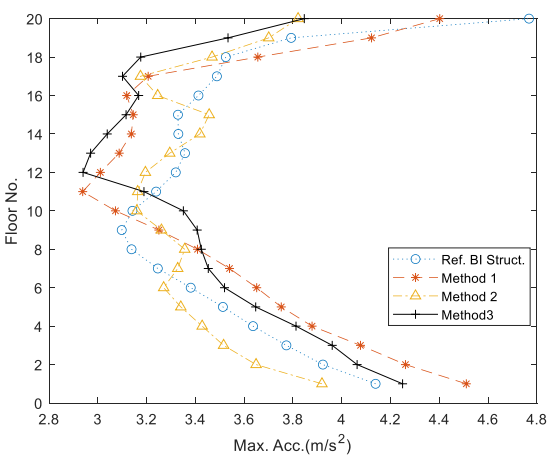


Fig. 8. Maximum floor accelerations for the reference BI structure and the base-isolated structures designed using methods 1, 2, and 3.

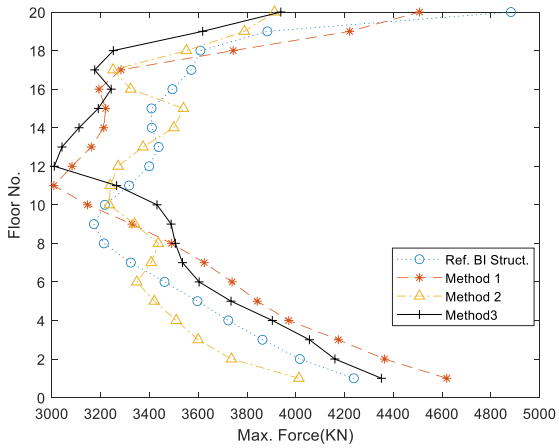


Fig. 9. Maximum floor forces for the reference BI structure and the base-isolated structures designed using methods 1, 2, and 3.

respectively. Similarly, the maximum floor acceleration in the reference BI structure is reduced to 4.40 m/s², 3.82 m/s², and 3.84 m/s² using methods 1, 2, and 3, respectively.

Figure 6 compares the maximum floor displacement values for the reference BI structure and the base-isolated structures designed using methods 1, 2, and 3. As shown, all three methods effectively reduce the maximum floor displacement, with the reduction being more pronounced on the upper floors of the studied structures. Method 1 demonstrates the best performance in reducing the seismic responses. Figure 7 presents the maximum floor drifts for the reference BI structure and the base-isolated structures designed using methods 1, 2, and 3. Methods 1 and 3 significantly reduce the maximum floor drift, particularly on the upper floors. Although method 2 does not perform as well in reducing the maximum drift on some lower floors, it effectively reduces the maximum drift on the upper floors.

Figures 8 and 9 compare the maximum floor accelerations and seismic forces of the reference BI structure and the base-isolated structures designed using methods 1, 2, and 3. The proposed methods reduce the maximum acceleration and seismic force on the upper floors of the studied structures. However, on the lower floors, there is a slight increase in these responses. It is important to note that even with this increase, the acceleration levels remain significantly lower than those in the FB structure and fall within the range of non-destructive floor accelerations. In conclusion, the advantages of the proposed methods in reducing maximum displacement and drift are achieved at the cost of a slight increase in maximum acceleration and seismic force on the lower floors.

The hysteresis loops of the seismic isolators in the reference BI structure and the base-isolated structures designed using methods 1, 2, and 3 are shown in Figure 10. There is no significant difference between the loops, indicating that the amount of dissipated energy by the seismic isolators in all four structures is nearly the same.

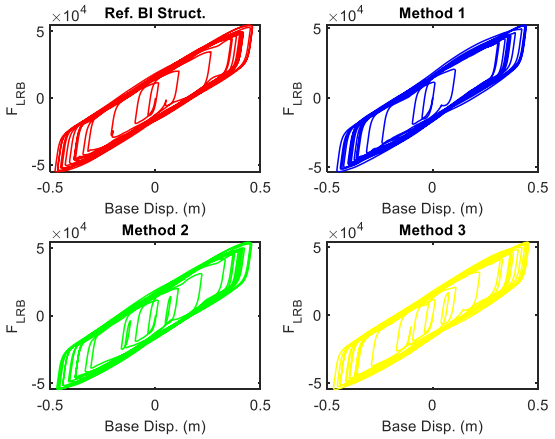


Fig. 10. Hysteresis loops of the seismic isolators for the reference BI structure and the base-isolated structures designed using methods 1, 2, and 3.

For further comparison, the reductions in seismic responses of the base-isolated structures designed using methods 1, 2, and 3, relative to the reference BI structure, are illustrated in figures 11, 12, 13, and 14. These figures respectively show the reduction percentages in maximum floor displacement, maximum floor drift, maximum floor acceleration, and maximum seismic force in comparison with those given for the reference BI structure. Figure 11 shows that method 1 results in a 5% to 14% reduction in maximum floor displacement, providing the best performance among the methods in reducing this response. Although the other methods also reduce maximum floor displacement, method 1 is the most effective. The efficiency of the proposed methods is particularly evident in reducing maximum floor drift, as shown in Figure 12. While the reduction is less pronounced on the lower floors, there is a significant 30% to 80% reduction in maximum drift on the upper 10 floors of the studied structures. This is crucial, as major structural and non-structural damages during earthquakes are often caused by large relative displacements between floors. Figures 13 and 14 demonstrate that the proposed methods result in a bit of reduction in maximum floor acceleration and seismic force on the upper floors of the studied structures, although there is a bit increase in these responses on the lower floors. However, it is important to note that the maximum floor accelerations remain within a range that is considered non-destructive.

To provide a general assessment of the seismic performance of the proposed methods, the average reductions in seismic responses, compared to the reference BI structure, are summarized in Table 2. These reductions are reported in terms of maximum floor displacement, maximum floor drift, maximum floor acceleration, and maximum seismic force. Overall, method 1 delivers the best performance, achieving reductions of 6.65%, 32.65%, and 0.88% in maximum floor displacement, drift, and acceleration, respectively, relative to

the reference BI structure. Although methods 2 and 3 show.

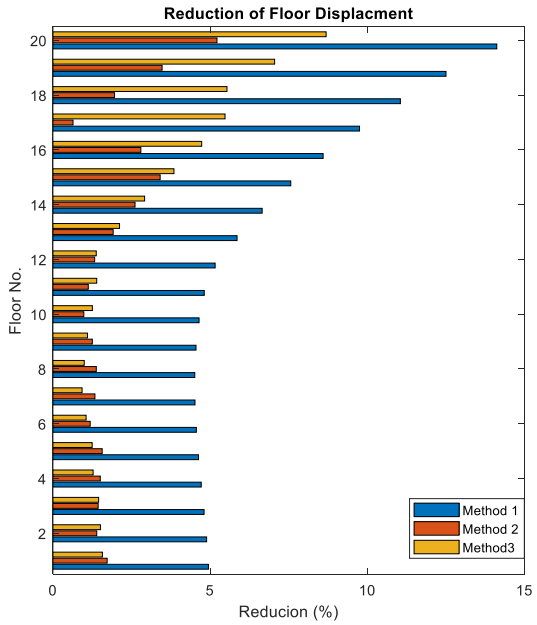


Fig. 11. The reduction percentages in maximum floor displacement for the base-isolated structures designed using methods 1, 2, and 3.

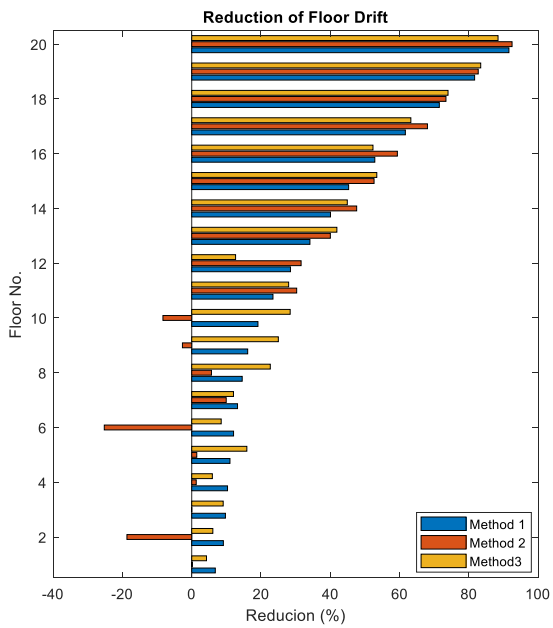


Fig. 12. The reduction percentages in maximum floor drift for the base-isolated structures designed using methods 1, 2, and 3.

only minor reductions in displacement and acceleration, they perform well in reducing the critical seismic response of maximum floor drift.

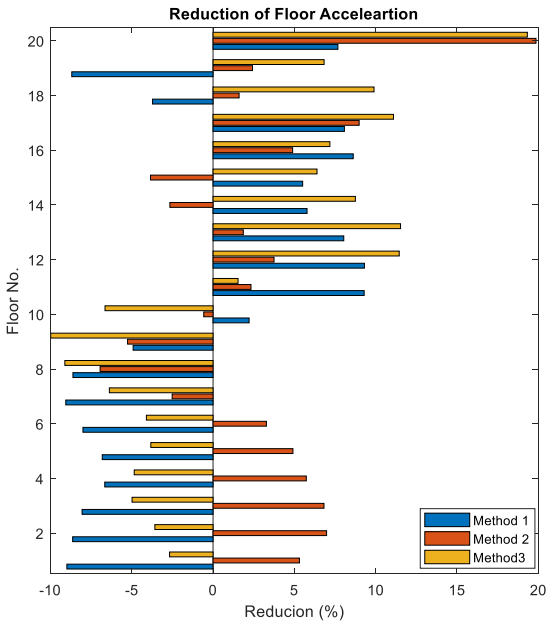


Fig. 13. The reduction percentages in maximum floor acceleration for the base-isolated structures designed using methods 1, 2, and 3.

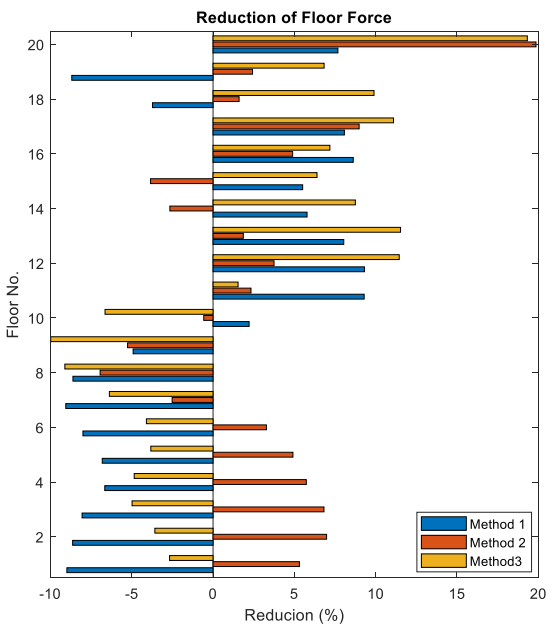


Fig. 14. The reduction percentages in maximum floor force for the base-isolated structures designed using methods 1, 2, and 3.

II. Conclusions

The seismic performance of base-isolated tall structures is often influenced by the superstructure's response and the relative lateral movements between its floors. In such cases

TABLE 2 THE AVERAGE REDUCTIONS IN SEISMIC RESPONSES

Seismic responses	Average reductions (%) in Method 1	Method 2	Method 3
Max. Disp.	6.65	1.91	2.78
Max. Drift	32.65	27.091	34.02
Max. Acc.	0.88	2.85	1.89
Max. Force	0.88	2.85	1.89

the effectiveness of seismic isolation in controlling inter-story drift and absolute acceleration of the floors is typically diminished. However, it is possible to regulate the superstructure's deformations by optimally designing floor stiffness through an optimization process aimed at achieving uniform deformation of the superstructure. This approach can create an optimal isolation condition where the superstructure behaves like a rigid body. In this study, three techniques were proposed to enhance the seismic performance of base-isolated tall buildings by promoting uniform deformation of the superstructure. Numerical analyses were performed on a 20-story base-isolated building, and the seismic performance of these techniques was evaluated and compared. The key findings are as follows:

1. All three methods effectively reduced maximum floor displacement, particularly in the upper floors. Method 1 achieved the best results, with reductions ranging from 5% to 14%.
2. These methods significantly minimized maximum floor drift, a critical seismic response. Methods 1 and 3 were notably successful, with reductions of 30% to 80% in the upper floors. While Method 2 was less effective on some lower floors, it still delivered significant reductions in the upper floors.
3. The proposed methods also achieved a 10% to 15% reduction in maximum acceleration and seismic forces on the upper floors. However, there was a slight increase in these responses on the lower floors, though they remained within non-destructive limits.
4. Method 1 provided the most consistent performance, achieving reductions of 6.65%, 32.65%, and 0.88% in maximum floor displacement, drift, and acceleration, respectively, compared to the reference base-isolated structure. Although Methods 2 and 3 showed only modest reductions in displacement and acceleration, they were highly effective in significantly reducing maximum floor drift, which is the most critical seismic response of the structure.

References

[1] F. Naeim, *Design of Seismic Isolated Structures: from theory to practice*: John Wiley & Sons, 1999.

[2] C. Ma, Y. Zhang, P. Tan, and F. Zhou, "Seismic response of base-isolated high-rise buildings under fully nonstationary excitation," Shock and Vibration, vol. 2014, p. 401469, 2014.

[3] H. Anajafi, K. Poursadr, M. Roohi, and E. Santini-Bell, "Effectiveness of seismic isolation for long-period structures subject to far-field and near-field excitations," Frontiers in Built Environment, vol. 6, p. 24, 2020.

[4] P. C. Roussis and M. C. Constantinou, "Uplift-restraining friction pendulum seismic isolation system," Earthquake engineering & structural dynamics, vol. 35, pp. 577-593, 2006.

[5] T. Ariga, Y. Kanno, and I. Takewaki, "Resonant behaviour of base-isolated high-rise buildings under long-period ground motions," The Structural Design of Tall and Special Buildings, vol. 15, pp. 325-338, 2006.

[6] J. Hino, S. Yoshitomi, M. Tsuji, and I. Takewaki, "Bound of aspect ratio of base-isolated buildings considering nonlinear tensile behavior of rubber bearing," Structural Engineering and Mechanics, vol. 30, pp. 351-368, 2008.

[7] C. Ma, Y. Zhang, P. Tan, and F. Zhou, "Seismic response of base-isolated high-rise buildings under fully nonstationary excitation," Shock and Vibration, vol. 2014, p. 401469, 2014.

[8] A. Nakai, D. Sato, T. Murakami, and K. Kasai, "Evaluation of stiffness of base-isolation layer and superstructure of high-rise baseisolated building based on seismic observation recording," AIJ J. Technol, vol. 24, pp. 571-576, 2018.

[9] A. Q. Darwish and M. Bhandari, "Seismic response reduction of high rise steel-concrete composite buildings equipped with base isolation system," Materials Today: Proceedings, vol. 59, pp. 516-524, 2022.

[10] Z. Li, G. Huang, X. Chen, and X. Zhou, "Seismic response and parametric analysis of inter-story isolated tall buildings based on enhanced simplified dynamic model," International Journal of Structural Stability and Dynamics, vol. 22, p. 2240008, 2022.

[11] S. Shourestani, F. Soltani, M. Ghasemi, and S. Etedali, "SSI effects on seismic behavior of smart base-isolated structures," Geomechanics & engineering, vol. 14, pp. 161-174, 2018.

[12] S. Pal, A. Hassan, and D. Singh, "Optimization of base isolation parameters using genetic algorithm," Journal of Statistics and Management Systems, vol. 22, pp. 1207-1222, 2019.

[13] S. Etedali, K. Hasankhoie, and M. R. Sohrabi, "Optimal design of pure-friction isolators with and without restoring device: A multi-objective cuckoo search-based approach for seismic-excited structures," in Structures, 2020, pp. 708-719.

[14] A. Ocak, S. M. Nigdeli, G. Bekdaş, S. Kim, and Z. W. Geem, "Optimization of seismic base isolation system

using adaptive harmony search algorithm," Sustainability, vol. 14, p. 7456, 2022.

[15] S. Öncü-Davas, R. Temür, and C. Alhan, "Comparison of meta-heuristic approaches for the optimization of non-linear base-isolation systems considering the influence of superstructure flexibility," Engineering Structures, vol. 263, p. 114347, 2022.

[16] S. Etedali and M. K. Kareshk, "Mitigation of torsional responses in asymmetric base-isolated structures using an optimal distribution of isolators in base story," in Structures, 2022, pp. 807-817.

[17] Y. Lei and X. Yang, "Stochastic Optimization of Electromagnetic Inertial Mass Dampers in Nonlinear Hybrid Base Isolation Systems Under Seismic Excitations," International Journal of Structural Stability and Dynamics, p. 2450241, 2023.

[18] S. Etedali and A.-A. Zamani, "Semi-active control of nonlinear smart base-isolated structures using MR damper: sensitivity and reliability analyses," Smart Materials and Structures, vol. 31, p. 065021, 2022.

[19] M. Abdechiri, M. R. Meybodi, and H. Bahrami, "Gases Brownian motion optimization: an algorithm for optimization (GBMO)," Applied Soft Computing, vol. 13, pp. 2932-2946, 2013.

[20] M. Shahi, M.R. Sohrabi, S. Etedali and A.A. Zamani, " Simultaneous optimal design of PID and MATMD considering their proposed elevation placement for seismic control of tall buildings on soft soil," International Journal of Industrial Electronics, Control and Optimization, vol. 6, pp. 241-259, 2023.

[21] S. Nagarajaiah and S. Narasimhan, "Seismic control of smart base isolated buildings with new semiactive variable damper," Earthquake Engineering & Structural Dynamics, vol. 36, pp. 729-749, 2007.

[22] A.A. Zamani, S. Tavakoli, S. Etedali, and J. Sadeghi, "Adaptive fractional order fuzzy proportional–integral–derivative control of smart base-isolated structures equipped with magnetorheological dampers," Journal of Intelligent Material Systems and Structures, vol. 29, pp. 830-844, 2018.

[23] S. Etedali, K. Hasankhoie, and M. R. Sohrabi, "Seismic responses and energy dissipation of pure-friction and resilient-friction base-isolated structures: A parametric study," Journal of Building Engineering, vol. 29, p. 101194, 2020.

[24] S. Etedali, "Sensitivity analysis on optimal PID controller for nonlinear smart base-isolated structures," International Journal of Structural Stability and Dynamics, vol. 19, p. 1950080, 2019.

[25] MATLAB. The Math Works, Inc., Natick, MA, 2000



Sadegh Etedali received his Ph.D. in Structural Engineering from the University of Sistan and Baluchestan, Zahedan, Iran, in 2014. He is currently an Associate Professor in the Department of Civil Engineering at Birjand University of Technology. Dr. Etedali has published over 100 scientific papers in national and international journals and conference proceedings. He has supervised/advised more than 20 M.Sc. and Ph.D. students. In recognition of his contributions to the field, he was listed among the top 2% of most influential scientists by Stanford University in both 2022 and